ELSEVIER

Biophysical Chemistry 53 (1994) 45–56

Biophysical Chemistry

Location of diphenyl-hexatriene and trimethylammonium-diphenyl-hexatriene in dipalmitoylphosphatidylcholine bilayers by neutron diffraction

Eva Pebay-Peyroula [a,*], Erick J. Dufourc [b], Arthur G. Szabo [c]

[a] *Institut Laue Langevin, Avenue des Martyrs, B.P. 156X, 38042 Grenoble Cedex, France*
[b] *Centre de Recherche Paul Pascal, CNRS, Avenue A. Schweitzer, 33600 Pessac, France*
[c] *Institute for Biological Sciences, NRCC, Ottawa, Ont., Canada, K1AOR6*

Received 15 October 1993; revised 10 January 1994; accepted 15 January 1994

Abstract

Neutron scattering experiments have been performed on oriented dipalmitoylphosphatidylcholine (DPPC) bilayers containing diphenylhexatriene (DPH) or its trimethylammonium analog (TMA-DPH). DPH and TMA-DPH were either protonated or deuterated in one of the phenyl rings which afforded by using proton–deuterium contrast methods the location of these fluorescent probes in the model membrane. Both probes exhibit bimodal distributions in DPPC. The position, population and orientation in the two sites vary depending upon the physical state of the bilayer (gel or fluid) and the presence or absence of the TMA group. In gel ($L_{\beta'}$) phase lipids DPH is located close and parallel to the bilayer surface (site I) and near the bilayer center, oriented at $\approx 30°$ with respect to the normal to the surface (site II). On going to the fluid (L_α) phase, a distribution of orientations around the parallel to the surface is only observed for site II. Orientation of DPH in site I is unchanged. In the gel phase TMA-DPH is found in a position close and parallel to the bilayer surface (site I) and in a position (site II) oriented at an angle of $\approx 25°$ with respect to the bilayer normal, with the trimethylammonium group anchored in the head group domain. On going to the fluid phase there is a change in molecular orientation of each of the sites. In site I the molecule penetrates deeper in the bilayer and adopts a $\approx 20°$ tilt with respect to the surface, with an orientational distribution of $\pm 10°$. In site II the molecule becomes perpendicular to the membrane surface. Changes in population of sites, both with DPH and TMA-DPH, are observed on going from low to high temperatures. They are however difficult to quantitate due to experimental conditions. The H_2O–^2H_2O exchange experiments afforded an estimate of the water layer thickness as well as the maximum penetration of water into the interior of the bilayer.

Keywords: DPH; TMA-DPH; Neutron-diffraction; Deuterated-probes; Model membrane

1. Introduction

Most of our understanding of the dynamics and structure of biological membranes relies on techniques such as vibrational spectroscopy (IR, Raman), magnetic resonance (NMR, EPR) and fluorescence for the dynamics, and X-ray diffraction for the structure. Some

Abbreviations: IR = infrared; NMR = nuclear magnetic resonance; EPR = electron paramagnetic resonance; DPH = 1,6-diphenyl-1,3,5-hexatriene; TMA-DPH = 1-[4-(trimethylammonium)phenyl]-6-phenyl-1,3,5 hexatriene; DPPC = 1,2-dipalmitoylphosphatidylcholine

* Corresponding author.

SSDI 0301-4622(94)00075-U

of these are probe techniques which monitor the molecular order and dynamics of extrinsic molecules embedded in the membrane structure. The structural and dynamical properties of fluorescent lipid probes in membrane systems are considered to reflect the structural order and dynamics of the acyl chains surrounding them. Time-dependent fluorescence decay and fluorescence anisotropy measurements are a convenient means of studying acyl chain lipid structure and dynamics, provided that the reorientational motions of the probe molecules take place on the timescale of the intrinsic fluorescence decay. 1,6-diphenyl-1,3,5-hexatriene (DPH) and its polar analogue, 1-[4-(trimethylammonium)phenyl]-6-phenyl-1,3,5-hexatriene (TMA-DPH) have been used extensively in such fluorescence measurements owing to several favourable properties [1,2]. Both molecules, especially DPH, are insoluble in aqueous buffers. Hence they both associate with lipid bilayers, and it has been thought that DPH partitions into the acyl chain hydrophobic core of membranes. On the other hand TMA-DPH is thought to be anchored with the positively charged trimethylammonium group in the lipid water interface and the phenylhexatriene portion in the acyl chain interior, perhaps at a lesser depth than DPH itself. The exact location of these probes in the lipid bilayer and membrane has largely been inferred from solubility properties, effects of dielectric constant on their spectroscopic properties, and their cylindrical shape. In truth their localization and orientational distribution in the lipid bilayer has not been structurally defined, especially in the fluid phase.

It has been recently shown that the analysis of time-resolved fluorescence anisotropy from these two probe molecules in lipid bilayer membranes was not straightforward [3]. The anisotropy decay data was best fit by a model where the DPH exhibits a bimodal orientational distribution with respect to the bilayer surface. Ameloot et al. [4] report that TMA-DPH is located at a site which is nearly parallel to the bilayer normal. There are now a number of recent reports which suggest that these fluorescent lipid probes, especially DPH, are heterogeneously distributed in membranes [5–8]. Straume and Litman [9] in their time resolved fluorescence study of DPH and TMA-DPH in unsaturated acyl chain lipid vesicles concluded that there was a bimodal distribution of DPH in these vesicles and that increasing the temperature or degree of insaturation of the acyl chains resulted in an orientational redistribution of DPH. One of these distributions was that with the long axis of DPH aligned along the bilayer normal. The other site which was occupied by a considerable proportion of the DPH was oriented parallel to the bilayer plane, orthogonal to the first site, and in the interfacial region of the bilayer.

The goal of the present work is to determine the location of these fluorescent probes in a bilayer membrane, by means of a completely different technique, i.e. neutron diffraction experiments. Protonated and deuterated DPH and TMA-DPH molecules were successively embedded in membranes in order to take advantage of the difference in sign and magnitude of the coherent scattering amplitudes of these two hydrogen atom isotopes. It has been already demonstrated [10–14], that the difference between Fourier profiles obtained from samples containing deuterated and undeuterated probes allows to locate, in real space, i.e. within the bilayer thickness, their accurate location. It is worthwhile mentioning that similar labelling experiments have been recently performed using X-ray diffraction with brominated lipid analogs or brominated cholesterol in lipid bilayers [15–17]. It has also been shown, from X-ray diffraction experiments, that fluorescent probes in lecithin bilayers perturb the bilayers [18]. Recently, a work was reported in which both X-ray and neutron diffraction experiments were used to refine the bilayer structure described as a number of quasimolecular components [19].

The model membrane used herein is dipalmitoylphosphatidylcholine (DPPC). Experiments have been performed below and above the temperature, T_c, of the gel-to-fluid phase transition, in order to monitor the effect of the physical state of the lipid membrane (ordered or disordered) on probe locations.

2. Experimental

2.1. Materials

Protonated DPH, TMA-DPH and DPPC were obtained from Sigma (France) and used without further purification. The fluorescent probes were deuterated in one of the phenyl rings, as shown in Figs. 4–7, according to procedures which will be published else-

where (A.G. Szabo, D.T. Krajcarski and L. Smith, manuscript in preparation).

2.2. Sample preparation

Oriented multilayers were prepared as follows. Lipids (30 mg), DPH and TMA-DPH were dissolved separately in chloroform. Solutions of the probe molecules were added to lipids in order to obtain 10 and 20 mole percent of the fluorescent probe with respect to DPPC. The relatively high concentrations of DPH (20%) and TMA-DPH (10%) were used for all experiments decribed herein in order to ensure a sufficient signal to give significant differences after subtraction (*vide infra*). The organic solvent was removed from the solution mixture by evaporation under nitrogen gas. Further solvent evaporation was performed under high vacuum for one hour. The dried mixture was then dispersed in a phosphate buffer (50 mM, pH = 7.0) and several freeze–thaw cycles coupled with mechanical shaking on a vortex mixer were performed in order to ensure sample homogeneity. Microscope slides (previously treated by overnight immersion in a chromic acid solution, washed and dried) were coated with the lipid dispersion and placed for 3 h in an oven (55°C, 75% humidity), to achieve sample annealing to form oriented multilayers.

This procedure was repeated for samples containing protonated or deuterated molecules. In order to determine the sign of the structure factors (*vide infra*), samples were also prepared with different heavy water contents in the buffer of 0, 50 and 100%.

2.3. Neutron diffraction

Diffraction experiments on the oriented samples were performed on the D16 neutron diffractometer at ILL. This instrument is installed on a cold neutron guide and a pyrolitic graphite monochromator selects a wavelength of 4.54 Å. The diffracted intensities are recorded on a two-dimensional ^{3}He detector. The samples were mounted on a goniometer placed in a sealed temperature-controlled can in the presence of an appropriate saturated NaCl bath to maintain constant relative humidity of 75% at both temperatures studied [20].

Diffraction peaks were measured by setting the center of the detector approximately to 2θ and by scanning the sample around the Bragg angle, θ, in a narrow angular range relatively to the mosaicity. The frames were recorded on a MicroVax II. A first integration was performed in the vertical direction, masking each frame in order to sum only the area under the peaks. The vertical peak width results from the convolution of the sample mosaic spread and the beam geometry (beam height and divergence), it increases with the peak order. Therefore less of the detector is masked for higher orders. For samples of a 10° mosaic spread, under usual experimental conditions (beam height of 2 cm and 0.4° of divergence), the vertical integration was performed on the central half of the detector for the first order. The mask size decreased progressively and the eighth order was measured with no masking. The different frames were then added together and a final integration of the Bragg peaks along the 2θ axis (angle between diffracted and direct beam), with background subtraction, yielded $I(h)$, i.e. the total integrated diffracted intensity versus h, where h is the order of the Bragg peak (Fig. 1). The lamellar spacings, d, were obtained by fitting the peak positions according to Bragg's law ($2d \sin\theta = h\lambda$).

The absolute values of the structure factors are related to the measured intensities in the following way [12]:

$$|F(h)| = [I(h)a(h)P(h)L(h)]^{1/2}\,\mathrm{corr}(h), \qquad (1)$$

where $a(h)$ is the absorption correction for a one-dimensional crystal, $P(h)$ is a geometric factor taking into account the amount of sample in the neutron beam, $L(h)$ is the Lorentz factor and finally $\mathrm{corr}(h)$ is a factor resulting from the method of integrating the intensities

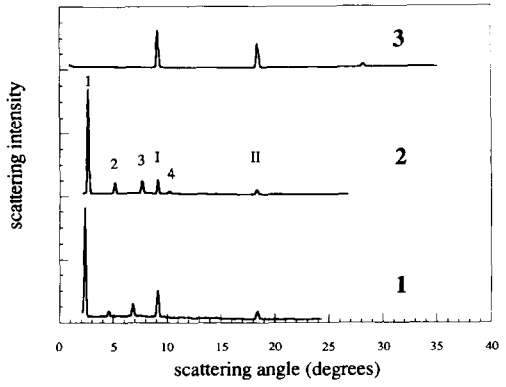

Fig. 1. Diffraction patterns $I(h)$ of oriented samples of: (1) DPPC with 20% DPH-$^2H_5$ at 26°C. (2) DPPC with 20% DPH-$^2H_5$ at 64°C. (3) pure DPH-$^2H_5$ crystals. 2θ is the angle between the direct and the diffracted beams. Neutron wavelength, $\lambda = 4.54$ Å.

which tends to underestimate the lower orders. The absorption correction for a one-dimensional crystal on a plate is [12]:

$$a(h) = 1/\{h[1 - \exp(-4\mu t d/h\lambda)]\}, \quad (2)$$

where μ is the attenuation factor (5 cm^{-1} for DPPC bilayers), t the thickness of the sample, d the lamellar spacing and λ the wavelength. $P(h)$ is a surface corrective factor for higher orders for which the sample does not entirely lay in the neutron beam. The Lorentz factor is $L(h) = \sin(2\theta)\sin\theta$ as for a powder type sample. Although the samples are oriented, they still have a notable mosaicity. As a result, the diffraction spots are spreading out vertically, increasingly with the Bragg angle. For the higher orders, the spots are larger than the detector height. To avoid truncation errors of the profile wings, the spots are integrated only over the maximum plateau of the profile using a mask which is different for each order. The vertical peak profile is the convolution of sample mosaicity, beam dimension and beam divergence. Our samples have mosaicities ranging from 5 to 10°: in such conditions, the profile of the first order is determined by the beam geometry while for the fourth order the mosaicity is predominant. The intensity plateau for the first order is thus diminished by the contribution of the beam profile. To take into account this underestimation of the first order, corr(h) is introduced, it varies linearly from 1.64 for $h = 1$ to 1.0 for $h = 10$. This factor is first experimentally determined with pure DPPC bilayers and can be described by a simple peak profile model where mosaicity and divergence are modelled by gaussian distributions and the beam profile by a square function (Pebay–Peyroula, unpublished results).

Since the sample structure is considered to be centrosymmetric, the phases of the structure factors are either 0 or π. It is known that in this case, the dependence of the neutron structure factors versus the ^2H_2O content in the water layer is linear for each order [21]. Thus the phase differences between two ^2H_2O concen-

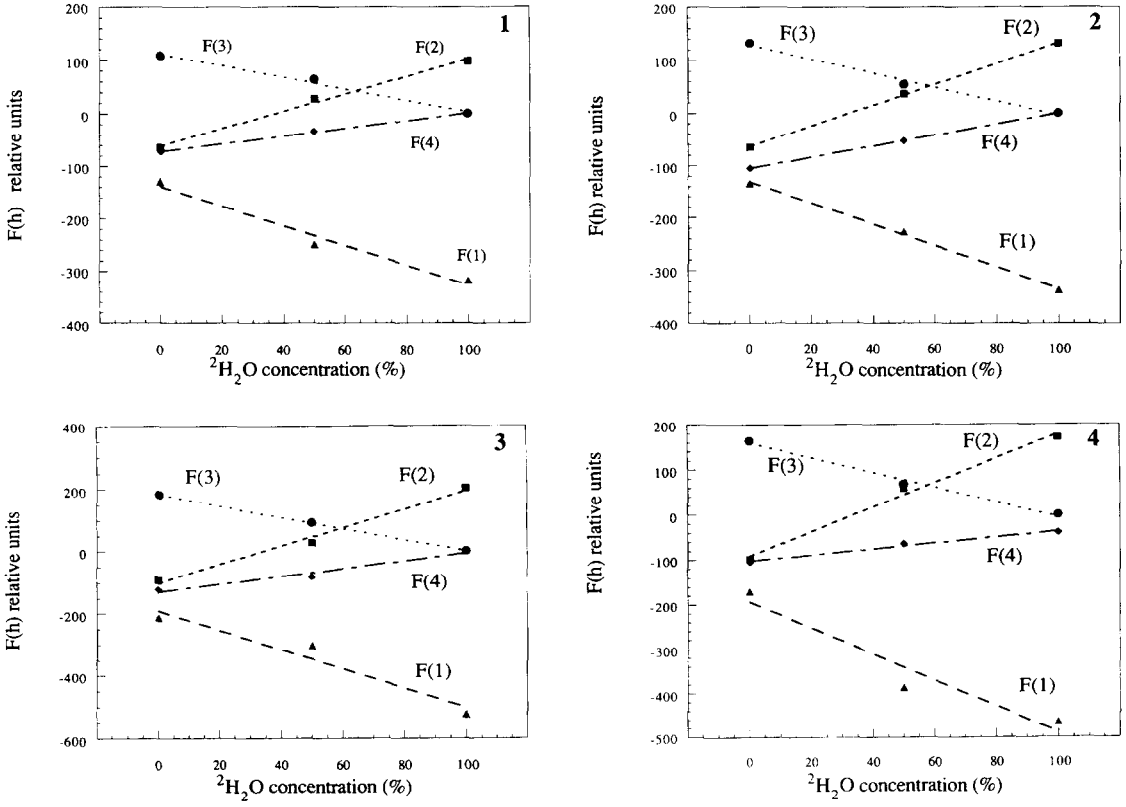

Fig. 2. Variation of structure factors, $F(h)$ versus ^2H_2O concentration. See text for details. (1) sample D at 26°C. (2) sample D at 64°C. (3) sample E at 26°C. (4) sample E at 64°C.

trations are obtained by collecting data for three contrasts: 0, 50 and 100% ^2H_2O and the relative signs of $F(h)$ are chosen such that $F(h)$ versus these concentrations are linear (Fig. 2). Two of the 0% phases are fixed, one by the choice of origin: the cell origin is fixed at the center of the bilayer, the other by choosing a positive scattering density difference between the headgroups and the bilayer center. Supplementary information is required for the determination of other phases, these were obtained from the difference profile between the same sample in 100% ^2H_2O and in 0% ^2H_2O. This difference profile only reflects the scattering of the water layer and should therefore correspond to a positive peak centered on $\pm d/2$, where d is the cell dimension [11].

Scattering profiles in real space are then derived from the Fourier transform of structure factors:

$$\rho(x) = 2/d \sum_h F(h) \cos(2\pi hx/d), \quad (3)$$

where x is the direction normal to the bilayer surface.

Specific positions can be labelled by chemical substitution of one or several protons by deuterons [12]. These substitutions are generally isomorphous, therefore the diffraction profile of the labelled position results from the difference between the labelled, $\rho_D(x)$, and the non-labelled, $\rho_H(x)$, profiles:

$$\rho_{label}(x) = \rho_D(x) - s\rho_H(x), \quad (4)$$

where s is an appropriate scaling factor. An absolute scaling for each sample was obtained from the water distribution profiles [11]. Profiles can be normalized by considering that the surface of the water peaks corresponds to the difference in scattering length of n ^2H_2O and n H_2O molecules, where n is number of water molecules per unit cell, which is otherwise known [22].

The label distribution profile was modeled by Gaussian distributions. More exactly the structure factors of the labels were fit to the structure factors of one or two Gaussian distributions. Instead of fitting the real space profile there are advantages in fitting the experimental to calculated structure factors from a model with Gaussian labels [12]. This has the advantage of minimizing considerably the truncation errors due to the low resolution. The scattering profile of one label is described by:

$$g(x) = (w_i/2\nu_i\sqrt{\pi})(\exp\{-[(x-x_{0_i})/\nu_i]^2\} + \exp\{-[(x+x_{0_i})/\nu_i]^2\}), \quad (5)$$

where x_{0_i} is the label position, ν_i is related to the distribution width ($\nu_i = \mathrm{FWHM}/2\sqrt{\ln 2}$) and w_i is the weight for label i. The structure factors in reciprocal space are:

$$F_c(h) = 2t_i w_i \times \exp[-(h\pi\nu_i/d)^2] \cos(2\pi h x_{o_i}/d), \quad (6)$$

where t_i is the extra scattering length of label i (scattering length difference between deuterated and hydrogenated label).

3. Results

3.1. Neutron diffraction patterns

Diffraction patterns were recorded for the following samples: DPPC (A), DPPC with 20% DPH (B), DPPC with 20% DPH-$^2H_5$ (C), DPPC with 10% TMA-DPH (D) and DPPC with 10% TMA-DPH-$^2H_5$ (E). Letters in parenthesis are the abbreviations for these samples in the following text. Each sample was examined in 75% relative humidity (obtained from a saturated NaCl solution), for two temperatures 26°C (gel phase, $L_{\beta'}$) and 64°C (fluid phase, L_α) and for three ^2H_2O concentrations (0, 50 and 100% ^2H_2O). NaCl was chosen because the relative humidity imposed by a saturated NaCl solution is nearly constant between 26°C and 64°C [20]. Significant intensities were obtained up to the fourth or fifth order. Figs. 1.1 and 1.2 show the diffraction pattern of sample C at 26°C and 64°C respectively. There are two sets of reflections. The set labelled 1, 2, ... are from the bilayer structure, the set labelled I, II, ... are from DPH crystals remaining in the sample as shown in Fig. 1.3. There is a superposition of a DPH crystal peak and the fourth order in sample C at 26°C. The crystalline dimension of DPH crystals is 14.5 Å, the vertical peak profile indicates that this dimension is parallel to the bilayer crystal axis. These crystal reflections are not affected by the temperature: the scattering profile (Fig. 1.3) is the same at 26°C and 64°C. As a consequence, the two contributions can easily be separated. The ratio of the two DPH-crystal peaks is estimated from a DPH crystal sample

Table 1
Diffraction intensities, $I(h)$, for DPPC in the presence and the absence of DPH and TMA-DPH

Sample [a]	h [b]	^2H_2O content (%)					
		$T=26°C$			$T=64°C$		
		0	50	100	0	50	100
A	1	4678		73035	9456		236049
	2	559		3043	457		13925
	3	707		0	913		0
	4	209		68	292		258
B	1	3382	7960	70350	9147	35772	204847
	2	895	3172	2982	348	147	11284
	3	861	0	0	804	563	0
	4	190	0	49	305	346	181
C	1	9175	14663	22664	13966	19453	110057
	2	411	113	330	1768	120	4906
	3	1186	190	100	2438	199	32
	4	2516 [c]	1795 [c]	1601 [c]	415	169	179
D	1	5182	18753	31220	14280	28930	86397
	2	375	71	890	774	72	3860
	3	543	188	0	1555	409	0
	4	151	34	0	436	198	0
E	1	5559	15992	34867	9092	47305	68110
	2	389	123	1594	892	328	2712
	3	825	142	0	1250	217	0
	4	328	82	0	321	121	46

[a] Sample composition: (A) DPPC, (B) DPPC with 20% DPH, (C) DPPC with 20% DPH-$^2H_5$, (D) DPPC with 10% TMA-DPH, (E) DPPC with 10% TMA-DPH-$^2H_5$.
[b] Diffraction order.
[c] These intensities result from the superposition of bilayer diffraction peak and crystalline DPH diffraction.

and from sample C at 64°C. Thus measuring the second peak of DPH-crystals in sample C at 26°C, we estimate the intensity of the first DPH-crystal peak. Subtracting this intensity from the measured intensity we could estimate $I(4)$ for sample C. The amount of DPH incorporated into the membrane in sample B and C was considered to be the same because of the identical way of preparing the sample. Evidence of small amounts of crystals in the samples was also seen in the TMA-DPH samples. The peaks resulting from TMA-DPH crystals are well separated from the bilayer peaks, leading to straightforward measurements of lamellar intensities. Table 1 summarizes the diffracted intensities for all the samples in different conditions of temperature and ^2H_2O content. The statistical errors on the intensities scale as $(N+B)^{1/2}/(N-B)$, where N is the total number of counts in the peak and B the number of background counts. Typically the statistical errors range from 1% to 2% for large peaks, 2% to 5% for medium peaks and the errors can go up to 30% for very weak peaks.

The lamellar spacings reported in Table 2 show no significant differences for pure DPPC samples nor for DPPC initially incubated with 20% DPH or 10% TMA-DPH at a given temperature. The same conclusion can be made regarding the thickness of the lipid bilayers because of the constant water thickness observed in the water profiles (see below). The change in spacing going from 26°C to 64°C is also the same for DPPC and DPPC containing the fluorescent probes, suggest-

Table 2
Structure factors and lamellar spacings for 0% ^2H_2O water content samples, in gel and fluid phases

Temp.	Sample [a]	$F(1)$	$F(2)$	$F(3)$	$F(4)$	d (Å)	a (cm Å^{-3}) [b]
26°C	A	−123	−78	+123	−84	58.0	1.95×10^{-17}
	B	−105	−99	+136	−80	58.7	1.89×10^{-17}
	C	−172	−67	+160	−130	58.2	2.00×10^{-17}
	D	−130	−64	+108	−72	59.0	3.00×10^{-17}
	E	−134	−65	+133	−105	58.6	2.60×10^{-17}
64°C	A	−173	−70	+140	−103	52.1	1.06×10^{-17}
	B	−170	−61	+132	−106	51.7	1.17×10^{-17}
	C	−211	−138	+229	−123	52.2	1.11×10^{-17}
	D	−213	−91	+183	−121	51.9	1.73×10^{-17}
	E	−170	−98	+164	−104	51.6	1.98×10^{-17}

Accuracy of d spacings is ±0.1 Å, accuracy on $F(h)$ ranges between 5% (large F values) to 15% (weak F values).
[a] Sample composition as in Table 1.
[b] a is a normalization factor (scattering length per unit volume) by which $F(h)$ has to be multiplied to obtain absolute $F(h)$ factors.

ing that the phase transition is not perturbed by the probes. Moreover, solid state deuterium NMR, using chain perdeuterated DPPC showed that the lipid phase transition and the chain order parameter profile were little affected by the presence of DPH (Dufourc, unpublished results). The presence of DPH and TMA-DPH crystals indicates that the concentration of fluorescent probes in the membrane is less than the 20% or 10% initially incubated during sample preparation. In fact, some control experiments performed with 2.5% fluorescent probe concentration led to comparable results (data not shown), supporting the results obtained at higher concentrations. The uncertainties on the lamellar spacings in Table 2, result from the standard deviations when calculating the spacing for each diffraction order. In fact, for each order the experimental error results from the wavelength dispersion (less than 1%) and the angular resolution (0.15°, using a sample to detector distance of 100 cm).

3.2. Phase determination and water distribution

Relative phases were obtained by plotting F(h) versus ^2H_2O concentration as shown in Fig. 2. The straight lines which are obtained are consistent with a centrosymmetric structure. The plots obtained for samples D and E are of very good quality at both 26°C and 64°C (Fig. 2). For sample B at 64°C and C at 26°C and 64°C the plots are of lesser quality but still acceptable. For sample B at 26°C, the 50% ^2H_2O sample was probably

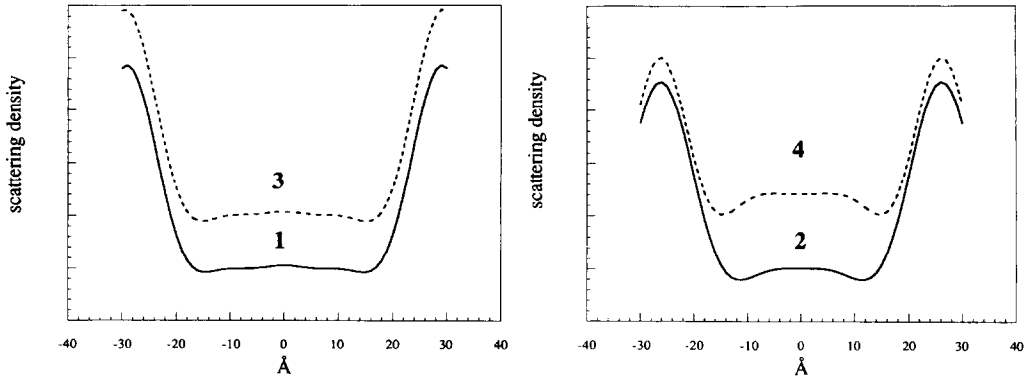

Fig. 3. Water distribution in model membranes. (1) in DPPC at 26°C. (2) in DPPC at 64°C. (3) in DPPC with 20% DPH at 26°C. (4) in DPPC with 20% DPH-$^2H_5$ at 64°C. The origin represents the bilayer center. The flat distribution inside the membrane shows that there is no water penetrating inside. The two peaks centered at $\pm d/2$ correspond to water layer.

not sufficiently equilibrated, i.e. the ^2H_2O exchange between the bilayer and the salt solution had not stabilized. The choice of the unit cell origin fixes one of the phases. The other phases are chosen such that the water profiles show peaks centered on $\pm d/2$ and a flat density between the peaks.

For each sample, the water profiles were obtained by subtracting the 0% from the 100% ^2H_2O profile. Fig. 3 shows the water scattering profiles for some samples. It is noteworthy that the width of the water layer is the same for all samples at a given temperature. Except for sample C at 26°C (for which the 100% ^2H_2O was probably not sufficiently equilibrated) all the water profiles show the correct flat profile at the bilayer center. A relative scaling can be obtained for all the samples by equating the areas of the water peaks [21]. In order to estimate the absolute scale, we consider a unit cell of surface S, and of volume $V = Sd$. For a DPPC bilayer at 20°C and 6% water content (obtained from a saturated LiCl salt solution), Tardieu and co-workers [22] have shown that the composition of the unit cell is five water molecules for two DPPC molecules and $S = 42.7$ Å^2. In their case the bilayer repeat distance was 57.7 Å, which is not very different from our repeat distance at 26°C. Therefore we felt justified in using the same unit cell composition and the same S value. The surface under the water peak (in one unit cell) is the difference in scattering length of five ^2H_2O and five H_2O molecules divided by the unitary surface S. This allows to determine the absolute scale for each profile.

The structure factors and lamellar spacings obtained for samples A, B, C, D and E at 26°C and 64°C in 0% ^2H_2O water content are shown in Table 2.

3.3. Diffraction profiles and label positions

The one-dimensional Fourier transform of the structure factors for each sample gives the corresponding diffraction profile. The difference between the ^2H-labelled sample and the non-labelled sample, gives the label position. The deuterated ring positions are presented for TMA-DPH in DPPC gel (Fig. 4) and fluid (Fig. 5) phases and for DPH in the same lipid in gel (Fig. 6) and fluid (Fig. 7) phases.

The peak positions observed from the scattering profiles in Figs. 4–7 can be modelled by Gaussian peaks, according to Eq. (5) [23]. The parameters (number of Gaussians, position, width and weight) are determined by comparing the experimental profile obtained from the measured intensities to the calculated profiles up to the fourth order. Unfortunately, this profile comparison cannot be obtained by a mathematical mini-

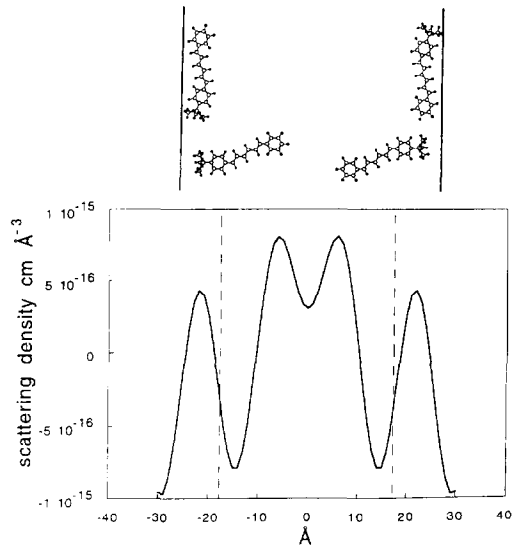

Fig. 4. (Bottom) Scattering profile for the labelled ring of TMA-DPH, in DPPC bilayers, at 26°C. Solid line: experimental data. Dashed line: calculation using a gaussian distribution with parameters of Table 3 (see text). The dashed vertical lines represent the lower limit for water penetration in the bilayer. (Top) Tentative representation of the TMA-DPH molecules in the lipid bilayer. The full circles represent the deuterated labels. The solid vertical lines represent the upper limit of the bilayer (choline head groups).

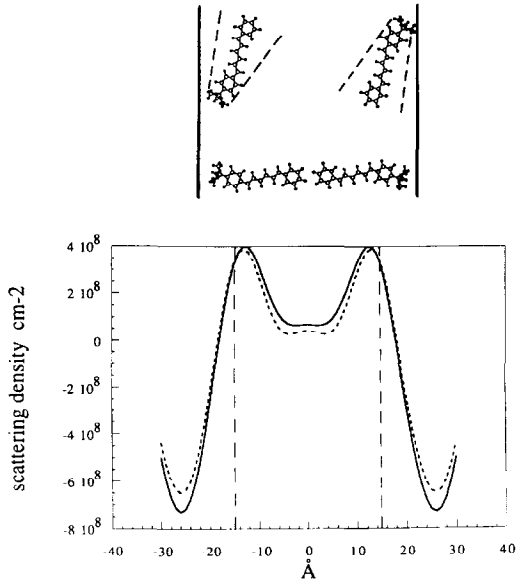

Fig. 5. Same as in Fig. 4, except $T = 64$°C.

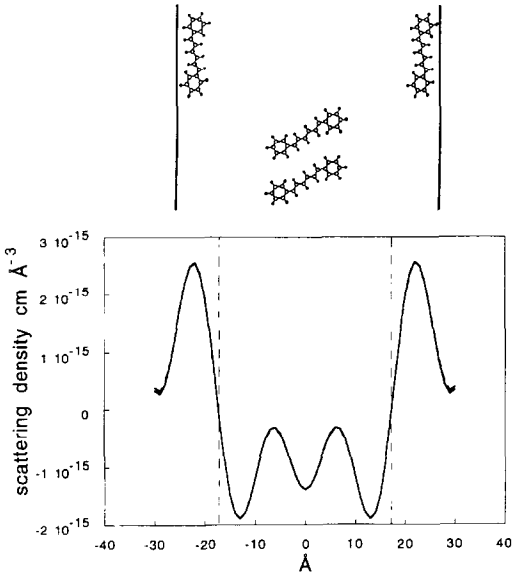

Fig. 6. (Bottom) Scattering profile for the labelled ring of DPH, in DPPC bilayers, at 26°C. Solid line: experimental data. Dashed line: calculation using a gaussian distribution with parameters of Table 3 (see text). The dashed vertical lines represent the lower limit for water penetration in the bilayer. (Top) Tentative representation of the DPH molecules in the lipid bilayer. The solid vertical lines represent the upper limit of the bilayer (choline head groups).

mization because the number of parameters (5 for two Gaussians) is larger than the number of experimental data (4 orders). The width of the experimental distribution is a convolution between the effective label distribution width in the sample and the experimental resolution. The experimental width is correlated to the occupancy and even with more experimental data it would not be significant to refine both values. Therefore the widths are fixed to a reasonable value (larger than 4 Å). The positions and the relative occupancies are fitted by minimizing the usual crystallographic R factor and by maximizing the correlation between the experimental and the calculated structure factors. All the label profiles were best fit by two Gaussian peaks (in the asymetric unit) with different widths and weights. Results of best fits are collected in Table 3 and the corresponding calculated profiles using four orders are shown (dashed line) by superimposition on the experimental ones in Figs. 4–7. The close correspondence between the model fitting and the experimental data gives confidence in the data treatment which involved scaling procedures for profile subtractions.

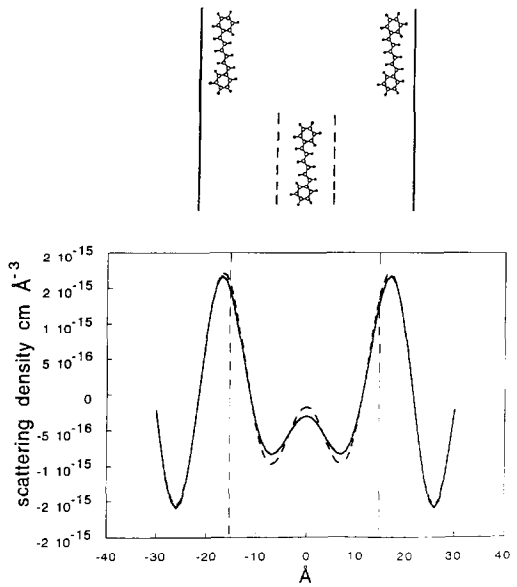

Fig. 7. Same as in Fig. 6, except $T = 64$°C.

4. Discussion

The peaks in Figs. 4–7 represent the positions of the deuterated rings, which allows to propose positions of the whole molecule in the different samples.

4.1. TMA-DPH

TMA-DPH, with a trimethylammonium group attached to one of the phenyl rings, has a positively charged group and therefore is expected to be anchored near the surface of the lipid bilayer, owing to electrostatic interactions. The deuterated phenyl ring is opposite to the TMA-attached ring. In the gel phase (Fig. 4), two ring positions are observed in a bilayer half. The profile can be fit according to Eq. (5) and gives a ring positioned at 21.6 Å (site I) and another at 5.7 Å (site II), relative to the bilayer center (0 Å). The width of the Gaussian distributions of the labels is 5 Å (Table 3). The drawing in Fig. 4 is an attempt to visualize the molecule locations of the probe in the bilayer. It must be emphasized here that the drawings represent ring positions for the average value of the Gaussian distribution, that is, the molecules occupy the shown position within ± 5 Å. The vertical lines represent the bilayer surface, i.e. the end of the phosphocholine head group. This representation shows the TMA group approxi-

Table 3
Model fitted locations of DPH and TMA-DPH deuterated rings

Site		DPH		TMA-DPH	
		26°C	64°C	26°C	64°C
I	position (Å)	23 ± 0.2	16.4 ± 0.4	21.4 ± 0.2	12.8 ± 0.2
	width (Å)	4	5	5	10
	weight	0.9 ± 0.2	0.8 ± 0.2	0.4 ± 0.05	0.9 ± 0.05
II	position (Å)	5.3 ± 0.5	0 ± 2	5.7 ± 0.2	2.6 ± 0.4
	width (Å)	4	8	5	5
	weight	0.1	0.2	0.6	0.1
correlation		99.9%	99.7%	100%	100%
R factor		1.4%	7%	0.2%	1.2%

Positions are expressed relative to the bilayer center (origin). Gaussian widths and weights correspond to ν_i and w_i of Eq. (5) (see text). The positions and the relative occupancy of one label were refined by maximizing the crystallographic *R* factor:

$$R = \sum_h ||F_{calc}(h)| - |F_{obs}(h)|| / \sum_h |F_{obs}(h)|$$

and maximizing the correlation between the $F_{obs}(h)$ and $F_{calc}(h)$. The steepness of the minima or maxima leads to the accuracy indicated in the table. Parameters without accuracy were not refined.

mately at the level of the phosphate and glycerol backbone groups. In site II, the molecule would be tilted by $\approx 25°$ relative to the bilayer normal, whereas site I would be required to lie parallel to the membrane surface. Orientation in site II is in agreement with the well known acyl chain tilt in the gel phase [24].

In the fluid phase (Fig. 5), a peak is observed at 12.8 Å from the origin (site I) and a plateau occurs in the bilayer center. This plateau can be accounted for by the superimposition of peaks (site II) very close to the origin. The calculation gives a peak position at 2.6 Å (Table 3). Site I has a width for the gaussian distribution of labels of 10 Å. The width of the gaussian distribution is larger than the average size of the deuterated phenyl ring (4–5 Å). This suggests that there is a distribution of locations around 12.8 Å. It is noteworthy that the distribution is larger than in the gel phase. Since the TMA group is considered to be anchored at the interface, this large distribution can tentatively be represented by a conical envelope for TMA-DPH in Fig. 5, top. The fluorophore in site I would then be tilted by $\approx 20°$ ($\pm 10°$) away from the bilayer surface. The second location (site II) in the fluid phase, is better localized as shown in Fig. 5. The TMA-DPH is then perpendicular to the bilayer surface, with the deuterated phenyl ring very close to the bilayer center.

4.2. DPH

Contrary to TMA-DPH, the DPH molecule is symmetric and it is supposed that the deuterated ring has no preferential position as compared to its hydrogen containing counterpart. Consequently, if a deuterated ring position is observed, there is also a hydrogenated ring in the same position and vice versa. Therefore, a given location for the DPH molecule is obtained by relating two peaks in Figs. 6 and 7. The distance between these two peaks may vary from 12 Å to 0 Å for molecules respectively parallel and perpendicular to the bilayer normal. The 12 Å is estimated from the barycenters of the two phenyl rings.

In the gel phase (Fig. 6) two peaks are observed at respectively 5.3 Å and 23 Å from the bilayer center (0 Å). Model fit locations according to Eq. (5) are done considering a 4 Å gaussian width for each label. These two peaks cannot be due to the same molecule, hence two DPH locations are needed to account for the profile. In site I, the fluorophore necessarily lies flat, parallel to

the surface (Fig. 6, top) whereas in site II, two locations could account for the observed profiles. Similarly to site I, the peaks at 5.3 Å relative to the bilayer center could be accounted for by molecules oriented parallel to the bilayer surface. Alternatively, molecules tilted by $\approx 30°$ with respect to the bilayer normal would also account for the peaks near the bilayer center. It seems that the second orientation is more probable since the tilt angle is comparable to that of the lipid chains in the $L_{\beta'}$ phase [24]. Furthermore with this angle and the length of DPH (12 Å), the two aromatic rings would correspond to the 5.3 Å and −5.3 Å peaks (Fig. 6).

In the fluid phase, two peaks are also observed (Fig. 7, bottom). As in the gel phase, these locations cannot be related to one molecule distribution only. Calculations give ring locations at 16.4 Å and 0 Å, the latter being at the bilayer center, for sites I and II, respectively (Table 3). Site I has a 5 Å gaussian width for the label. As for the gel phase the DPH molecule in this site would lie parallel to the membrane surface, (Fig. 7, top). Site II is characterized by its location at the bilayer center, nearly parallel to the surface. There is a 8 Å gaussian width for the label. As for the TMA-DPH molecule in the fluid phase (site I), the Gaussian width for DPH in site II is larger than the deuterated ring size, indicating a broader distribution of molecule orientations. Fig. 7, top illustrates this distribution by a domain (dashed lines) in which the DPH molecule would be found at the bilayer center. In this position, the molecule orientation would vary from 90° to 70° with respect to the bilayer normal. Attempts to fit the data to a distribution where there was a population of DPH with its long axis aligned with the acyl chains was not satisfactory. This orientation at the bilayer center in the fluid phase is a most controversial proposal, but is the only one consistent with the data.

Table 3 also reports on relative populations of molecules in each of the sites. We would like to emphasize here that caution must be taken in the interpretation of populations or temperature-driven population changes of DPH and TMA-DPH in the two sites. The fluorophore containing samples indeed showed little but marked presence of non adsorbed crystals of DPH or TMA-DPH. Although these contributions can easily be substracted from the bilayer diffraction, the small bilayer insoluble excess of fluorophore could alter the population distribution of molecules in the bilayer. As a consequence, the populations of sites as given in Table 3 must be regarded as rough estimates. Nevertheless it appears that the amount of DPH in site I (near the bilayer surface) is predominant and independent of temperature. For TMA-DPH the population of both sites is about the same in the gel phase and changes on going to the fluid phase where the location roughly parallel to the surface (site I) dominates.

It is interesting to note that a bimodal distribution function for DPH orientations in bilayers was proposed in order to account for time resolved fluorescence anisotropy data [25–27]. Our results are consistent with such a proposal. However, there is a marked concentration difference of fluorescent probes in the membrane between neutrons and fluorescence experiments. In order to draw a parallel between the two sets of measurements one should idealy repeat the neutron experiments with a lower concentration of fluorophore in the bilayer. However the neutron scattering is not strong enough to really perform the experiment.

The neutron diffraction data allows to estimate the penetration water depth into the bilayer interior. Fig. 3 indicates that there is some population of water to a depth of 17 Å and 15 Å on each side of the bilayer center for the DPPC gel and fluid phases, respectively. The deepest water penetration in the bilayer is represented by a vertical dashed line in Figs. 4–7. On the other hand, it is known that the fluorescence decay of DPH is markedly affected by the dielectric constant of the surrounding medium [28–30]. In polar solvents a lower fluorescence intensity and concomitantly shorter decay times are observed. As a consequence, the majority of the fluorescence would be due to molecules in the bilayer interior (site II).

The above rationalization indicates that care is required in the interpretation of fluorescence data of these probes in lipid bilayers. In studies of membranes where the surface bound water may be affected, i.e. dehydrated by extrinsic bound proteins or metal ions [31,32] or where water can penetrate even further into the bilayer core owing to integral proteins, this could affect the distribution of sites and polarity of the probe environment. The data in this report show that the orientational distribution of the probes depend on the physical state of the lipid matrix, i.e. either ordered or disordered. Hence, it is expected that cholesterol which causes an ordering of the lipid matrix could lead to unimodal or at least reduced bimodal fluorescence decay behavior [25].

5. Conclusion

The use of neutron diffraction of protonated and specifically deuterated molecules embedded in oriented lipid bilayers demonstrated that the fluorescent probes DPH and TMA-DPH both exhibit a bimodal distribution function in DPPC bilayers. In addition, both the orientation and the populations of the two membrane sites vary with the physical state of the lipid membrane (gel or fluid). It is also found that these fluorescent probes have rather well defined positions in the ordered gel ($L_{\beta'}$) phase and show a broad distribution of locations in the less ordered fluid (L_{α}) phase. Moreover, determination of water penetration by proton–deuterium contrast methods allows to discuss which of the molecules in the various membrane sites may be active in fluorescence experiments.

Acknowledgements

The authors are grateful to Dr. G. Zaccai for very helpful advices and comments on the first draft of the paper. The very best technical assistance by J.M. Reynal is also warmly acknowledged. The synthetic assistance of D.T. Krajcarski and L. Smith (NRC Co-op student) is sincerely appreciated. Discussions with Dr. J. Drew regarding synthetic pathways were most helpful. Travel assistance for AGS was obtained from the CNRS-NRC Canada–France exchange program and is gratefully acknowledged.

References

[1] D.A. Barrow and B.R. Lentz, Biophys. J. 48 (1985) 221.
[2] F.G. Prendergast, R.P. Haugland and P.J. Callahan, Biochemistry 20 (1981) 7333.
[3] H. Van Langen, D. Engelen, G. van Ginkel and Y.K. Levine, Chem. Phys. Letters 138 (1987) 99.
[4] M. Ameloot, H. Hendrickx, W. Herreman, H. Pottel, F. van Cauwelaert and W. van der Meer, Biophys. J. 46 (1984) 525.
[5] B.W. Williams and C. Stubbs, Biochemistry 27 (1988) 7994.
[6] R.M.M. Fiorini, M., Valentino, S. Wang, E. Glasser and E., Gratton, Biochemistry 26 (1987) 3864.
[7] R.M.M. Fiorini, M. Valentino, E. Glasser, E. Gratton and G., Curatola, Biochim. Biophys. Acta 939 (1988) 485.
[8] E. Kalb, F. Paltauf and A. Hermetter, Biophys. J. 56 (1989) 1245.
[9] M. Straume and B.J. Litman, Biochemistry 26 (1987) 5113.
[10] D.L. Worcester, in: Biological membranes, Vol.3 (Academic Press, New York, 1976) ch. 1.
[11] G. Zaccai, J.K. Blasie and B.P. Schoenborn, Proc. Natl. Acad. Sci. USA 72 (1975) 376.
[12] G. Büldt, H.U. Gally, J. Seelig and G. Zaccai, J. Mol. Biol. 134 (1979) 673.
[13] S.H. White, G.I. King and J.E. Cain, Nature 290 (1981) 161.
[14] R.E. Jacobs and S.H. White, Biochemistry 28 (1989) 3421.
[15] M.C. Wiener and S.H. White, Biochemistry 30 (1991) 6997.
[16] T.J. McIntosh and P.W. Holloway, Biochemistry 26 (1987) 1783.
[17] N.P. Franks, T. Arunachalam and E. Caspi, Nature 276 (1978) 530.
[18] W. Lesslauer, J.E. Cain and J.K. Blasie, Proc. Nat. Acad. Sci. USA 69 (1972) 1499.
[19] M.C. Wiener and S.H. White, Biophys. J. 59 (1991) 174.
[20] M.A. O'Brien, J. Sci. Instr. 25 (1948) 73.
[21] D.L. Worcester and N.P. Franks, J. Mol. Biol. 100 (1976) 359.
[22] A. Tardieu, V. Luzzati and F.C. Reman, J. Mol. Biol. 75 (1973) 711.
[23] G. Zaccai, G. Büldt, A. Seelig and J. Seelig, J. Mol. Biol. 134 (1979) 693.
[24] M.J. Janiak, D.M. Small and G.G. Shipley, Biochemistry 15 (1976) 4575.
[25] H. van Langen, G. van Ginkel, D. Shaw and Y.K. Levine, Eur. Biophys. J. 17 (1989) 37.
[26] M.J.M. van de Ven and Y.K. Levine, Biochim. Biophys. Acta 777 (1984) 283.
[27] L. Best, E. John and F. Jähnig, Eur. Biophys. J. 15 (1987) 87.
[28] E.D. Cehelnik, R.B. Cundall, J.R. Lockwood and T.F. Palmer, Chem. Phys. Letters 27 (1974) 586.
[29] E.D. Cehelnik, R.B. Cundall, J.R. Lockwood and T.F. Palmer, J. Phys. Chem. 79 (1975) 1369.
[30] J.G. Kuhry, G. Duportail, C. Bronner and G. Laustriat, Biochim. Biophys. Acta 845 (1985) 60.
[31] G. Laroche, E.J. Dufourc, M. Pezolet and J. Dufourcq, Biochemistry 29 (1990) 6460.
[32] G. Laroche, E.J. Dufourc, M. Pezolet and J. Dufourcq, Biochemistry 30 (1991) 3105.